Sizing of Hybrid Energy Storage Systems using Recurring Daily Patterns

Shahab Karrari, *Member, IEEE,* Nicole Ludwig, Giovanni De Carne, *Senior Member, IEEE,* and Mathias Noe

***Abstract*—A hybrid Energy Storage Systems (ESS) consists of two or more energy storage technologies, with different power and energy characteristics. Using a hybrid ESS, both high-frequency and low-frequency power variations can be addressed at the same time. For an accurate sizing of a hybrid ESS, the use of high-resolution data is required. However, high-resolution data over long periods leads to large data sets, which are difficult to handle. In this paper, an improved motif discovery algorithm is introduced to find the most recurring daily consumption patterns within the time series of interest. The most recurring pattern is selected as the representative of the time series for sizing the hybrid ESS. Next, a simple optimization framework is proposed for selecting the cut-off frequency of a low-pass filter, used for allocating the power to different storage technologies. Finally, the proposed sizing approach is applied for sizing a hybrid battery-flywheel ESS at four different low voltage distribution grids in southern Germany using real measurement data. It is demonstrated that a hybrid ESS, with the characteristics derived from the most recurring patterns only, can effectively provide their intended grid services for most of the days during the whole period of the time series.**

***Index Terms*—Energy storage, Pattern recognition, Batteries, Flywheels, Motif Discovery, Sizing of energy storage systems.**

I. Introduction

THE increasing share of photovoltaic (PV) generation in low voltage distribution grids can lead to several challenges for distribution system operators. Due to the resistive nature of the grid at this voltage level, reverse power flows caused by excess PV generation can lead to voltage rise issues [1]. Furthermore, fast active power fluctuations, for instance, caused by passing clouds over the PV panels, can cause fast voltage changes, which can be a power quality issue according to the European grid code DIN EN 50160 [2]. These static and dynamic phenomena can limit the hosting capacity of a distribution grid for additional PV installations [1], [3].

A hybrid Energy Storage System (ESS), if sized accurately, can help tackle the aforementioned challenges in both the short and long term. A storage technology with a high energy density, such as Li-ion batteries, can store the surplus generation during noon in order to avoid reserve power flows and use it to reduce the evening demand peak, while a complementary storage technology with a high power density and high power cycling capability, such as supercapacitors or flywheels, can be used for continuously compensating the fast active power changes, and therefore, avoiding fast voltage fluctuations. For an accurate sizing of such storage systems, the use of measurement data from the point of connection is necessary. Sizing an ESS using historical measurement data in order to accommodate more and more renewables has been widely investigated in literature. Comparative reviews of these methods for various applications of energy storage systems can be found in [4] and [5]. For instance, in [6], a randomly selected daily power profile of a PV plant is used for sizing a hybrid supercapacitor-battery ESS.

When using measurement data to size an energy storage system, the data resolution and the time window of interest must be determined first. For sizing an ESS, the use of high-resolution data and including the entire frequency spectrum of the recorded power profile is highly recommended [7], [8]. This is especially the case for sizing a hybrid ESS, where a high power density ESS compensates for the high-frequency components of the power profile in the seconds range [9]. However, high-resolution data over a long horizon results in large data sets, which are difficult to work with. Such large data sets can drastically increase the computation time required for solving the sizing problem, and in the case of complex nonlinear optimization problems, it can make the problem intractable [10]–[12]. A common approach to avoid dealing with such large data sets is to select the power profile of a randomly selected day or period as the representative of the data set for the sizing study, often without a proper justification, as seen in [6], [7], [13]–[15]. However, this approach can lead to specific sizing outcomes and over- or underestimating the storage characteristics for the rest of the time series. Alternatively, authors in [16] have reduced the data resolution by converting 10-s data to 15-min values in order to ease the computational burden over a year, which eliminates the high-frequency components of the power profile, and therefore, is not applicable for a hybrid ESS. To properly find a representative power profile for the whole data set, clustering techniques, such as K-means clustering [10], [17], [18] or fuzzy C-means clustering [19] have also been used. Using a clustering approach, daily power profiles with similar features (e.g., peak and mean value) are grouped together, and the cluster centres are selected for the sizing study as the representative power profile. While this is a significant improvement to an arbitrary choice of a typical day, there are some limitations in using clustering techniques for such studies: since the daily power profiles are grouped together based on simple features such as their peak value, they are not necessarily similar. For instance, daily power profiles can have

This work was supported by the German Research Foundation (DFG) as part of the Research Training Group GRK 2153: Energy Status Data-Informatics Methods for its Collection, Analysis and Exploitation, the Germanys Excellence Strategy EXC number 2064/1 Project number 390727645, the Helmholtz Association within the Helmholtz Young Investigator Group "Hybrid Networks" (VH-NG-1613), and under the joint initiative "Energy System Design" in the Research Field Energy.

TABLE I
SUMMARY OF THE EXISTING APPROACHES FOR REDUCING THE DATA SIZE FOR SIZING STUDIES AND THEIR DRAWBACKS.

Literature	Used approach	Drawbacks
[6], [7], [13]–[15]	Arbitrary or unclear choice of a typical day or period	Can lead to over-sizing or under-sizing of the storage systems
[16]	Aggregation of high-resolution data into low-resolution data	Loss of high-frequency components of the power profiles
[10], [17]–[19]	Clustering algorithms (K-means and C-means)	1. Power profiles in one cluster are not necessarily similar. 2. Generate clusters with non-recurring power profiles. 3. Requires to specify the number of clusters beforehand. 4. Has been only applied to hourly data.

the same peak and mean value, while otherwise being entirely different. Moreover, clustering techniques also require the user to specify beforehand how many clusters the algorithm should find, which is often arbitrary to decide beforehand. Section I presents a summary of the existing approaches for reducing the data size for sizing studies and their drawbacks.

In [20], we have introduced a novel alternative for finding a representative power profile within the time series, where recurring daily consumption patterns are detected using a pattern recognition algorithm called *motif discovery* [21], and then used as input for the sizing study. Motif discovery has several advantages in comparison to the state-of-the-art clustering techniques. First, it uses random projection [22], which makes it faster than clustering approaches [23]. Moreover, it aims to find similar patterns by using the Symbolic Aggregated Approximation (SAX) of the data, rather than the data itself or its features, which helps to find similar (and yet not the same) patterns and reducing the effects of noise and minor power deviations in finding recurring patterns. Lastly, motif discovery does not need the additional step of finding optimal cluster parameters. In this paper, we extend the method presented in [20] in the following ways:

- The motif discovery algorithm has been improved by using Dynamic Time Warping (DTW), which helps to allocate the optimal alignment given two time-dependent sequences.
- An optimization framework has been introduced for decoupling the power profile to different energy storage technologies. The proposed approach has then been applied for sizing a hybrid battery-flywheel ESS in several low voltage distribution grids.
- The proposed sizing approach has been applied to four different power profiles with rather divers characteristics, measured at four low voltage distribution grids in southern Germany. The studied power profile reflect different PV penetration levels and type of consumers, which are used to show the generality of the prosed sizing approach.
- The effect of cut-off frequency of the filter for power decoupling in the hybrid ESS and choosing patterns other than the most recurring one on the sizing outcome has been studied and presented.

The remainder of this paper is organized as follows. The measured input data used for the sizing study are presented in Section II. In Section III, the proposed sizing methodology, including the improved motif discovery algorithm, an analysis of the derived standard patterns, and the optimization framework used for power allocation are described. The sizing outcome and the effect of different influencing factors such as the data aggregation and cut-off frequency of the low-pass filter are presented in Section IV. Finally, an evaluation of the proposed sizing approach using the standard patterns is given in Section V, followed by the conclusions given in Section VI.

II. THE INPUT MEASUREMENT DATA

The sizing calculations in this work are performed using the measured power profiles recorded at four different 10/0.4 kV substations in an area in southern Germany during July to September in 2018. The data has been collected in this period, in order to include a high PV generation level in the sizing study. The selection of these four substations is based on their relative voltage sensitivity to active power changes, estimated using the method proposed in [24]. The data has been recorded with different resolutions, starting from 1 second, using the "PQI-DA Smart" measurement device from the company A-Eberle [25]. The measurement device was installed at the low voltage side of the substation transformer to measure the total power of all the feeders supplied by each substation and to size a centralized ESS at the substation. Due to the high resolution of the data and limited storage capacity, two weeks of data has been collected at each substation.

Fig. 1 shows an example of 8 days of measurement at the four buses, starting and ending with a Monday. It can be seen that at each location, a daily consumption pattern is being repeated each day with slight variations, especially on weekdays. Bus 1 and 2 show a different pattern on weekends (6^{th} and 7^{th} day), as they mainly supply industrial and commercial customers. Bus 3 and 4 show similar patterns also during the weekends, as they are located in residential areas. Although these patterns seem similar, they are not identical. These buses represent different types of low voltage grids with different PV generation levels. Moving from bus 1 to 4, the share of PV generation increases, leading to reverse power flows during several days at bus 3 and 4, while this happens only during weekends for bus 1 and 2.

The power profiles at each bus also differ in terms of their frequency components. The one-sided frequency spectrum of the active power measurements in one week at the four buses using the discrete fast Fourier transform is shown in Fig. 2. Each power profile has different amplitudes at each frequency. For instance, while the power profile at bus 4 shows a significant amplitude at 0.0231 mHz, which corresponds to 12 hours, this value is much smaller for bus 3. This can also be seen in Fig. 4(d), where each day can be divided into two similar patterns. The frequency component at 0.0116 mHz, which corresponds to every 24 hours, can indicate daily recurrence of the pattern, which is higher for bus 3 and 4.

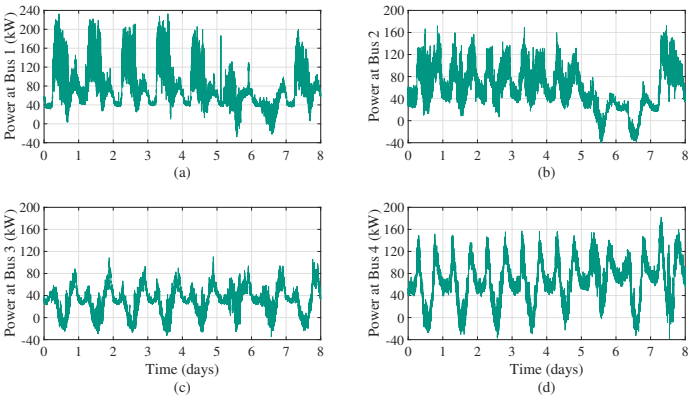

Fig. 1. The active power measurements at (a) bus 1, (b) bus 2, (c) bus 3, and (d) bus 4, for a period of 8 days, starting from Monday, which makes the 6th and 7th day, weekends. The data is shown with a 1-s data resolution.

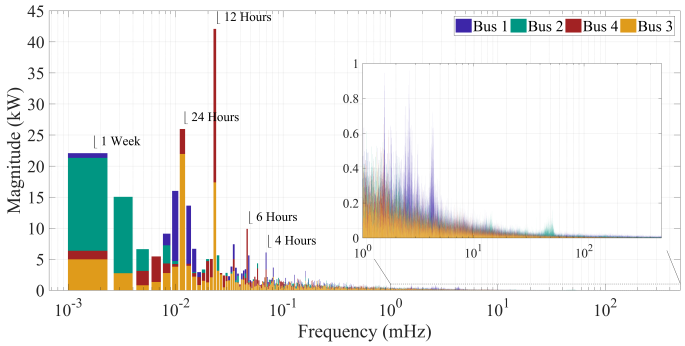

Fig. 2. Frequency spectrum of the power at the four buses in the period of one week using the 1-s data.

III. The Proposed Sizing Methodology

Fig. 3 shows the flowchart of the proposed sizing methodology, which consists of two main steps. In the first step, the improved motif discovery algorithm is applied to the measured time series in order to detect the most recurring pattern at each substation. In the second step, the derived patterns at each location are decoupled using a low-pass filter to allocate the power profiles of each storage technology. The cut-off frequency of this low-pass filter is determined through an optimization algorithm using the gradient search method. In the following, each of these steps is described in more detail.

A. Motif discovery using eSAX

Motif discovery is a pattern recognition method that has been used in different disciplines for applications such as seismology [26], classifying heart sounds [27], and more recently in the realm of electricity time series, to find flexibility potentials in industrial processes [28]. The standard motif discovery algorithm [21] searches for equal length time series sub-sequences which are similar. Thus, several similar sub-sequences form a motif. In this paper, we introduce Energy Time Series Motif Discovery using Symbolic Aggregated Approximation (eSAX), adapted to the needs of energy-related time series, and explained in detail in the following. The core innovation in Motif Discovery, in general, is the transformation

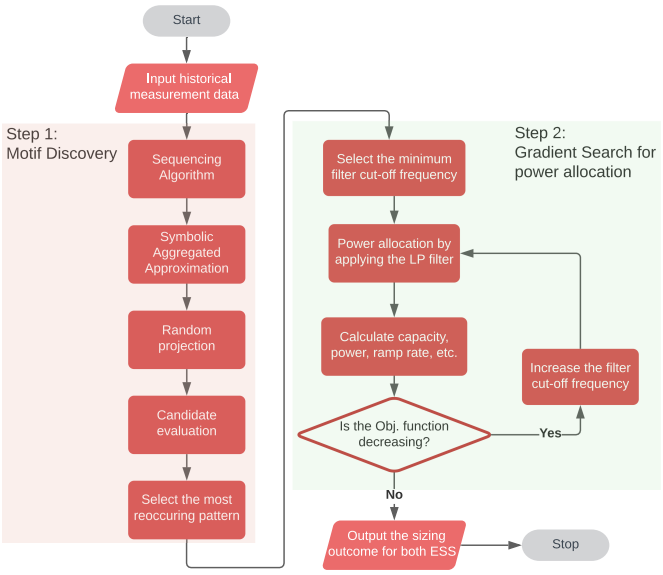

Fig. 3. The flowchart of the proposed sizing strategy.

of a time series into symbols, which reduces the noise and minor variations in the raw time series through approximations. Additionally, eSAX improves the previous Motif Discovery algorithm used in [20] by using a different distance measure and more flexible words.

The eSAX algorithm consists of five steps, as shown in Fig. 3. We start eSAX with a sequencing algorithm to find the sequences of interest, which we compare later for their similarity. These sequences can be of any length but are chosen to be an entire day (24 hours) in our case in order to find the daily power profiles. Given the sequences, we can then transform them into symbolic aggregated approximations. We do this through a piece-wise approximation of the time series, where the whole time series is approximated by the mean of different short pieces. These pieces can be any size in $[1, m]$, where m is the length of the sequence, and thus the aggregated time series will be at least of length one and at max at a length of m. As we compare different aggregations of the raw time series in this paper, we choose the piece size to be one, thus not having any form of approximation at this algorithm level. To arrive at a symbolic representation (SAX), each piece gets described by one letter. This letter comes from a predefined alphabet of length a, and a list of breakpoints β determines which piece is assigned which letter. The β parameters are based on the quantiles of the empirical cumulative distribution function, which for observations $x = (x_1, x_2, \dots x_n)$ is defined as

$$F_n(p) = \frac{1}{n} \sum_{i=1}^{n} \mathrm{I}(x_i \leq p). \tag{1}$$

For the next step, the random projection, the SAX representation of all sequences (i.e., the words) are saved row-wise in a *similarity matrix* S^*. In every iteration of the random projection algorithm, we randomly select l of the w columns of S^*, where l is a user-defined mask length, w is the word length and $l \leq w$. The word built with l columns is compared

to all $(n-m+1)$ rows of S^*. If there exists a match between the letters in the mask, the corresponding entry in the so-called *collision matrix* is incremented. The entries with the highest values in the collision matrix are considered candidate motifs. These motifs are transformed back to their piece values and then iterated over the original time series to calculate the distance to the raw sequences. Thus, finding the occurrences of the motif is the fourth step, the candidate evaluation. The distance measure used for the iteration is dynamic time warping (DTW), which finds the optimal alignment given two time-dependent sequences. Hence, for the sequences y_i and y_j of length n and m, DTW will align the two sequences with the help of a $n \times m$ matrix. In this matrix, every element contains the distance between two points from the sequence y_i and y_j, i.e., $d(y_i(a), y_j(b)) = (y_i(a) - y_j(b))^2$. This matrix is then used to find an optimal warping path through the distance matrix, where we want to find the path that minimizes the warping cost

$$\mathrm{DTW}(y_i, y_j) = \min \left\{ \sqrt{\sum_{k=1}^{K} w_k} \right\}, \tag{2}$$

with w_k defined as the k-th element of the warping path w. In contrast to Euclidean distances used in [20], this distance measure can also accommodate slight shifts in between two time series, such as slight time shifts in the peak demand in this use case. At the end of this fourth step, we are left with motifs containing several sequences.

B. The Derived Standard patterns

With the fifth and last step of our improved motif discovery algorithm (eSAX), we derive the most recurring consumption pattern at the four different low voltage distribution grids, described in Section II. In our use case using the 1-s data, between one motif and three motifs were found for each time series, covering most of the days within the original time series. The standard pattern is then defined as the 80% quantile of the detected motifs, and all motifs are shown in Fig. 4 using the 1-s data for the four substations. As seen from the standard patterns, bus 1 represents a low voltage feeder with industrial consumers with a low share of photovoltaic generation. On the other hand, bus 2 has enough PV generation to cover the increase in demand during midday, while for bus 3 and 4 the PV generation can cover the load entirely at times and cause reverse power flows.

To understand the effects of different types of loads and also the PV generation on the power profile in the frequency domain, a time-frequency analysis on the standard patterns is carried out, and the results are illustrated in Fig. 5. These spectrums are calculated using the short-time Fourier transform, and a *hamming* window with the length of 1 minute with no overlaps on standard patterns derived from the 1-s data. As seen in Fig. 5(a), the high-frequency components for bus 1 start and end with the beginning and end of the regular working hours, except for the lunch break around noon. In case of a high share of PV generation, as in buses 3 and 4, the power of the frequency components of both high- and low-frequency components become more volatile with the increasing PV generation during noon. Moreover, the constant power lines on the spectrum change from being horizontal to vertical, which means that the PV generation alters a relatively wide range of frequencies simultaneously. With the decrease in the PV generation, the frequency spectrum is restored, and the power profile contains the same frequency components as before the PV generation.

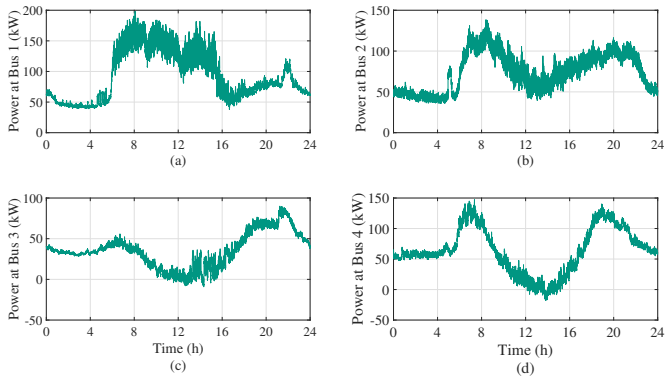

Fig. 4. The standard consumption patterns at the four buses. (a) Bus 1: No PV generation. (b) Bus 2: Limited PV generation to cover the base demand at peak generation. (c) Bus 3: Significant share of PV generation, capable of covering demand for short instance at peak generation. (d) Bus 4: High share of PV production, leading to slightly negative power flow at peak generation.

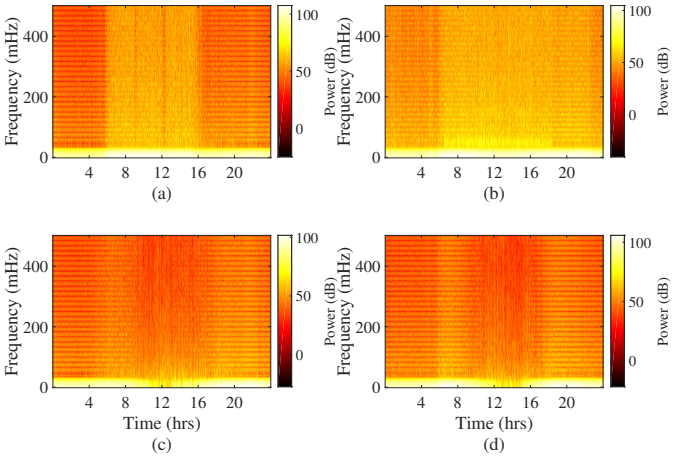

Fig. 5. The time-frequency analysis of the detected standard patterns using the short-time Fourier transform and a hamming window with the length of 1 minute with no overlaps on standard patterns at (a) bus 1, (b) bus 2, (c) bus 3 and (d) bus 4. At bus 1, there is an increase in the power of most frequency components within the working hours, except at lunch break around 12:00. At bus 3 and 4, the effect of PV generations can be clearly observed around noon.

C. Deriving the Storage characteristics

From the standard patterns derived using the motif discovery algorithm, the characteristics of a hybrid battery-flywheel ESS are calculated for each bus. The battery-flywheel ESS has been chosen as the storage solution in this paper, as a recent study has shown that a battery-flywheel hybrid system outperforms a battery-supercapacitor system in terms of the overall system efficiency and the reducing the peak current drawn from the battery [29]. The hybrid ESS, installed at the

substations, aims to flatten the consumption profile during the day at each location, while the main grid covers the average daily consumption. The residual power after deducting the daily average $P(t)$ is selected as the power profile that the hybrid ESS has to cover. The flywheel covers short-term power variations, while the Li-ion battery compensates for the power fluctuation in the long term. The following describes how the storage characteristics are calculated from the allocated power profile.

1) Nominal power: The nominal power ($\mathrm{P_n}$) for a converter-interfaced ESS is often limited by the converter ratings. The rated power can be calculated by simply applying the one-way efficiency of the ESS (η), considering both charging and discharging operation modes, and calculating the maximum value, as shown in (3) and (4). The *sign* function (sgn) is used to determine whether the ESS is being charged or discharged from the power profile for applying the system efficiency. It is assumed that the ESS has the same efficiency during both charging and discharging modes. The system one-way efficiency is assumed to be 90 % [30], which incorporates the efficiency of the converters and the storage medium. A safety margin can be added to (4), when necessary, in order to include larger daily peak variants.

$$R(t) = \eta^{-sgn(P(t))} P(t), \tag{3}$$

$$\mathrm{P_n} = \max |R(t)|. \tag{4}$$

2) Nominal capacity: The required nominal capacity ($\mathrm{E_n}$) determines the number of cells in a Li-ion battery and the maximum rotational speed and the inertia in a flywheel. The nominal capacity can be estimated by integrating over the power profile of the ESS and calculating the maximum change in the resulted variations in energy, as shown in (5) and (6).

However, for extending the lifetime of an ESS, particularly in the case of the Li-ion battery, oversizing is a common practice. For Li-ion batteries, it has been shown that avoiding high State of Charge (SOC) values can significantly help reduce the cells' cathode degradation and calendar ageing of the cells [31]. Similarly, deep discharging can significantly increase the internal resistance of the cells. Therefore, it is recommended to reserve a specific non-usable capacity for preventing high and low values of SOC, $\mathrm{SOC_{min}}$ and $\mathrm{SOC_{max}}$. Therefore, the nominal capacity can then be calculated using

$$E(t) = \eta^{-sgn(P(t))} \int_0^t P(\tau)\, d\tau, \tag{5}$$

$$\mathrm{E_n} = \frac{\max E(t) - \min E(t)}{\mathrm{SOC_{max}} - \mathrm{SOC_{min}}}. \tag{6}$$

The minimum and maximum SOC for sizing the Li-ion battery is assumed to be 10 % and 90 %, respectively, as suggested in [31]. These values for a flywheel are chosen to be 25 % and 100 %, respectively. This is due to the fact that while there is no upper limit in fully charging the flywheel, reaching low rotational speeds is often avoided in order to stay within the torque limits of the electrical machine [32].

3) Maximum ramp rate: The maximum ramp rate ($\mathrm{R_n}$) is calculated from the maximum difference between two consecutive points in the power profile of each ESS. Therefore, by assuming $\mathrm{f_s}$ to be the sampling frequency of the data,

$$\mathrm{R_n} = \max\left(|R(t) - R(t - \frac{1}{\mathrm{f_s}})|\right). \tag{7}$$

4) Number of mode changes: Since an ESS is not fully charged or discharged at each time of use, in this work, the number of mode changes from charging to discharging is calculated for each day instead of calculating the number of full cycles. Thus, the number of mode changes equals the number of *zero crossings* of allocated power profiles to each ESS.

D. Selecting the cut-off frequency for power allocation

A common approach for simultaneously sizing different storage technologies is using a Low-pass Filter (LPF) to decouple the allocated power profile's low- and high-frequency components. However, while the choice of the cut-off frequency of the LPF can significantly affect the sizing outcome [6], [33], there is no common approach for determining this value. Standard market intervals [34], typical discharge times of different storage technologies [20], [35], and optimization frameworks for minimizing the system costs [7] have been used previously for selecting the filter's cut-off frequency. If a relatively low cut-off frequency is chosen, the flywheel will cover most short-term power variations, but this choice also increases its nominal capacity. Increasing the capacity of a flywheel can be quite costly due to its high capital costs per unit of energy [36]. On the other hand, if a relatively high cut-off frequency, near half of the data sampling rate (the Nyquist frequency), is selected, the Li-ion battery will have to cover most of the fast changes, compromising any potential advantages using the flywheel.

In this work, a simple optimization framework is introduced for selecting the cut-off frequency of the LPF, which is based on the following assumptions:

1) Increasing the capacity of a flywheel is more costly than increasing the capacity of the battery [36].
2) Due to the higher power density of a flywheel, increasing its power ratings is preferred to the battery, as it requires less footprint.
3) It is desired to limit the ramp rate of batteries for a prolonged lifetime [31], while a high ramp rate is not a concern for flywheels.

With the aforementioned assumptions, an Objective Function (OF) is defined according to (8), which aims to minimize the capacity of the flywheel and maximize its power while reducing the maximum ramp rate expected from the battery.

$$\begin{aligned} \min_{f_c} \quad & OF = \mathrm{c_1} \frac{\frac{\mathrm{E_{n2}}}{\mathrm{E_{n1}}}}{\max(\frac{\mathrm{E_{n2}}}{\mathrm{E_{n1}}})} + \mathrm{c_2} \frac{\frac{\mathrm{P_{n1}}}{\mathrm{P_{n2}}}}{\max(\frac{\mathrm{P_{n1}}}{\mathrm{P_{n2}}})} + \mathrm{c_3} \frac{\frac{\mathrm{R_{n1}}}{\mathrm{R_{n2}}}}{\max(\frac{\mathrm{R_{n1}}}{\mathrm{R_{n2}}})} \\ \text{s.t.} \quad & 0 \leq f_c \leq 0.5\mathrm{f_s} \end{aligned} \tag{8}$$

In (8), index 1 refers to the characteristics of the Li-ion battery, while index 2 refers to the characteristics of the FESS.

TABLE II
THE OPTIMUM CUT-OFF FREQUENCY OF THE LPF FOR THE FOUR BUSES.

Bus No.	f_o (mHz) – 1-s data	f_o (mHz) – 1-min data
Bus 1	59	3.4
Bus 2	56	3.2
Bus 3	50	3.5
Bus 4	46	3.2

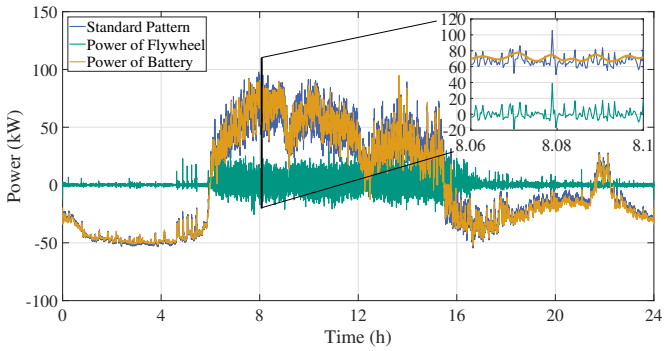

Fig. 6. The allocated power to each type of ESS at bus 1 by applying a low-pass filter with the optimum cut-off frequency of 59 mHz.

The nominal capacity, the nominal power, and the maximum ramp rate are calculated based on (3)-(7) for each cut-off frequency. The coefficients c_1-c_3 are weighting coefficients, which are assumed to be equal to one for the initial analysis. Following the aforementioned assumptions, the optimization framework of (8) aims for simultaneously minimizing the ratio of the capacity of the flywheel to the capacity of the battery, the ratio of the power of the battery to the power of the flywheel, and the ratio of the maximum ramp rate of the Li-ion battery to the one of the flywheel. These three factors are normalized using their maximum value. Using relative ratios as suggested here, instead of the common economic optimization frameworks [7], has the advantage that fixed cost values are not used, which can vary in time differently for each storage technology [37], and differ depending on the storage manufacturer [30]. It also avoids estimating the economic benefits of extending the battery's lifetime by reducing its ramp rate, which is difficult to quantify, as it depends on several external factors such as temperature.

To find the optimum cut-off frequency of the LPF (f_o), a simple gradient search is applied, similar to [33], in which the filter's cut-off frequency is increased stepwise from its minimum value as long as the objective function is decreasing. The cut-off frequency, at which (8) is no longer decreasing, is selected for decoupling the standard patterns, which are given in Table II for the four studied low voltage distribution grids using the 1-s and 1-min data.

As an example, Fig. 6 shows the decoupled power profile at bus 1 using the 1-s data after applying the LPF with optimum cut-off frequency. It can be seen that most short-term power variations are covered by the flywheel, such as the 40 kW pulsed power load connected just after 8:00, while the Li-ion battery only has to cover the slow variations in power.

IV. SIZING OUTCOME

After applying the LPF with the optimum cut-off frequency to the standard patterns derived using the motif discovery algorithm, the characteristics of the hybrid ESS can be calculated using (3)-(7). Table III shows the outcomes of the proposed sizing approach for the four studied low voltage distribution grids.

If we take the sizing outcome for bus 1 using the 1-s data as an example, it can be seen that the Li-ion battery has to provide a maximum ramp rate of only 4.84 kW/s, while the flywheel provides a maximum ramp rate of approximately 35 kW/s. Without the flywheel, the Li-ion battery has to provide the higher ramp rates continuously. Therefore, it can be concluded that the use of the flywheel also significantly reduces the number of times the Li-ion battery goes from charging to discharging modes and vice versa. Similar results were obtained for the other three buses. The maximum ramp rate and the number of mode changes are plotted in Fig. 7 for easier comparison.

It can also be observed from Table III that for buses 3 and 4, which are residential areas with a high share of PV generation, a smaller flywheel is needed with a capacity less than 1 kWh, a lower ramp rate and a smaller number of mode changes, when compared to bus 1, which supplies a small-scale industrial facility, reflecting the higher power variability in industrial processes, in comparison to residential consumption. In other words, the power fluctuations caused by PV generation units are in the lower frequency ranges, in comparison to the ones caused by industrial loads.

In the following subsections, the impact of several influencing factors on the sizing outcome is investigated.

A. The effect of cut-off frequency of the LPF

The storage characteristics given in Table III were calculated based on the optimum cut-off frequency derived from the proposed optimization framework. Fig. 8 shows the changes in the characteristics of both storage technologies if values other than the optimum cut-off frequency were selected for the power allocation at bus 1, as an example. Similar results can be shown for the other three buses.

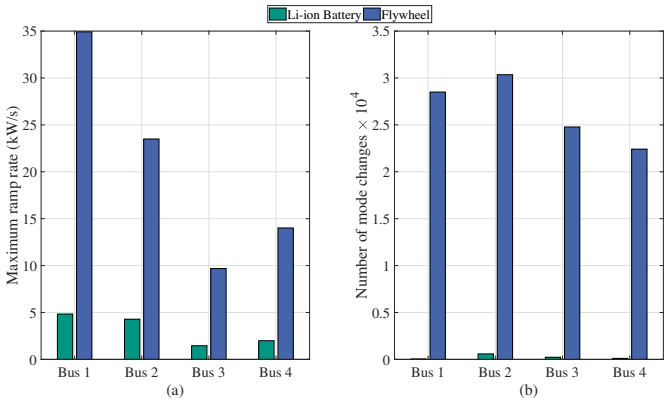

Fig. 7. (a) The maximum ramp rate, and (b) the number of mode changes per day for Li-ion battery and the flywheel using the 1-second data.

TABLE III
CHARACTERISTICS OF THE HYBRID BATTERY-FLYWHEEL ESS DERIVED FROM THE STANDARD PATTERNS.

Bus No.	ESS Type	Data Resolution	Capacity (kWh)	Nominal Power (kW)	Ramp Rate (kW/s)	Mode changes per Day
Bus 1	Li-ion Battery	1 s	615.32	94.87	4.84	34
		1 min	632.09	84	0.31	8
	Flywheel	1 s	1.99	38.94	34.92	28500
		1 min	2.47	20.75	0.46	813
Bus 2	Li-ion Battery	1 s	268.94	63.82	4.29	584
		1 min	219.23	70.09	0.26	46
	Flywheel	1 s	0.94	24.64	23.50	30352
		1 min	0.67	8.13	0.21	848
Bus 3	Li-ion Battery	1 s	268.53	56.96	1.46	226
		1 min	212.64	46.35	0.13	22
	Flywheel	1s	0.28	9.35	9.69	24780
		1 min	0.70	7.59	0.17	895
Bus 4	Li-ion Battery	1 s	450.5	87.34	1.99	106
		1 min	421.20	76.32	0.12	12
	Flywheel	1s	0.38	11.41	14.01	22415
		1 min	0.90	8.96	0.25	588

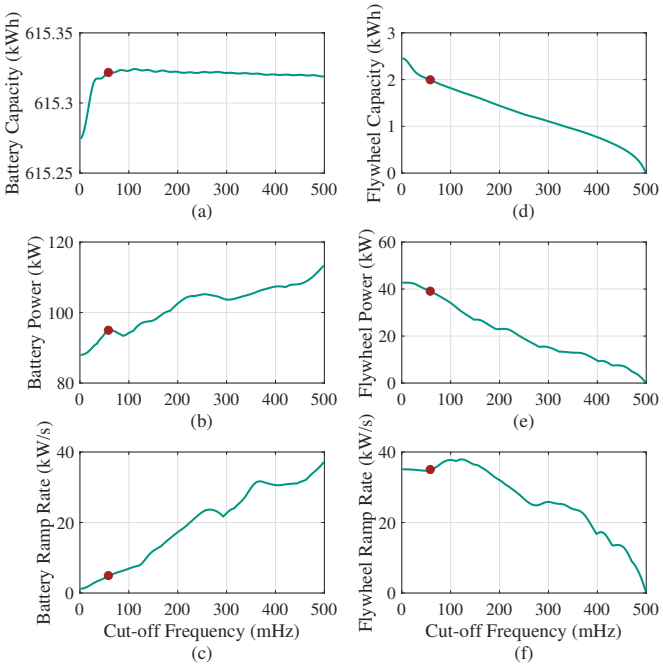

Fig. 8. The effect of increasing the cut-off frequency of the LPF at bus 1 on the characteristics of the Li-ion battery and the flywheel, when using the 1-s data. The optimum cut-off frequency is shown with the red marker.

As seen in Fig. 8, with the increase in the cut-off frequency of the LPF, the maximum ramp rate and rated power of the Li-ion battery increases, while its rated capacity remains relatively unchanged. On the contrary, higher cut-off frequencies decreases the capacity for the flywheel drastically, up to reaching zero at the Nyquist frequency (half of the sampling rate), where no power is being allocated to the flywheel. The optimum cut-off frequency, shown with the red marker in Fig. 8, is where the required capacity for the flywheel is relatively low (below 2 kWh for bus 1), while the required ramp rate of the Li-ion is also low (only 4.84 kW/s), which can potentially extend its lifetime.

The weighting coefficients c_1-c_3 in (8) can also be adjusted in order to give more priority to a certain ratio. For instance, if the single aim of the hybrid structure is to reduce the maximum ramp rate of the Li-ion battery using the flywheel for extending its effective lifetime, c_1 and c_2 can be set to zero, while $c_3 = 3$. This assumption leads to a flywheel energy capacity of approximately 2.4 kWh for bus 1, which is a 20 % increase from the calculated flywheel capacity using the equal weighing coefficients, leading to a significantly more storage costs. Alternatively, the limiting the capacity of the flywheel can become a higher priority, by increase the weighting coefficient c_2. In case of $c_2 = 2$, while $c_1 = c_1 = 0.5$, the flywheel capacity is reduced to 1.4 kWh, but at the price of the battery having to provide a ramp rate of 18 kW/s.

B. The effect of selecting other motifs

For the sizing outcome of Table III, the most recurring patterns have been used for the storage sizing. However, when using data with lower resolution or using longer time series, the motif discovery algorithm may find more than one recurring pattern with different number of recurrences. In our case studies, using the 1-s data, only one pattern has been detected. However, when using the 1-minute data, three different patterns were detected by the motif discovery algorithm at bus 2. This is a major advantage of the proposed approach in comparison to the state-of-the-art clustering techniques, where the number of clusters have to be defined before running the algorithm. But the motif discovery algorithm automatically finds how many repeating patterns are existing within time series. Bus 2 represents a low voltage distribution grid with small industrial/commercial customers. The three motifs when using 1-minute data for bus 2 are shown in Fig. 9, in the order of their number of recurrences. Pattern 1 is the most recurring profile for a typical workday, which has been used in this paper for the sizing calculations in Table III. Pattern 2 shows the power profile during the weekends and public holidays, in which PV generation is dominant in comparison to the peak demand, while pattern 3 represents the power profile of the first working day after weekends or holidays. The difference can be related to the loads that stay connected during the workdays but are disconnected for weekends and holidays.

TABLE IV
CHARACTERISTICS OF THE HYBRID BATTERY-FLYWHEEL ESS USING THREE DIFFERENT PATTERNS AT BUS 2 USING THE 1-MINUTE DATA.

Bus No.	ESS Type	Pattern	Capacity (kWh)	Nominal Power (kW)	Ramp Rate (kW/s)	Mode changes per Day
Bus 2	Li-ion Battery	1	219.23	70.09	0.26	46
		2	207.44	41.92	0.13	18
		3	408.87	74.33	0.17	28
	Flywheel	1	0.67	8.13	0.21	858
		2	0.60	9.61	0.30	826
		3	0.72	10.80	0.27	883

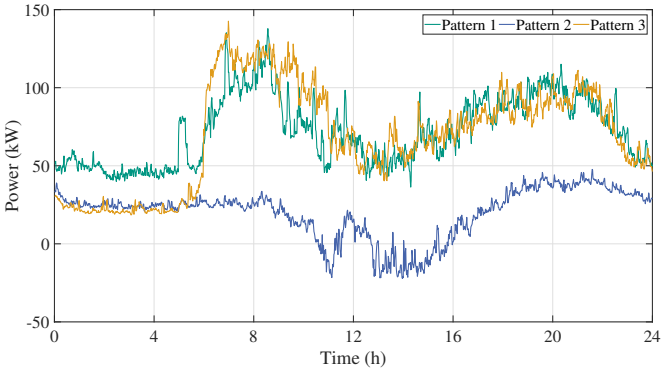

Fig. 9. The three different patterns detected by the motif discovery algorithm for bus 2 using the 1-min data in order of their number of recurrences.

The sizing outcome when using the three different patterns for bus 2 is shown in Table IV. It can be seen that when using pattern 2, which is the recurring pattern during weekends and holidays, the nominal power of the battery is largely underestimated (almost half), so the battery will not be able to handle the power profiles during weekdays. When pattern 3 is selected, which is the standard power profile for the first working day of the week, the battery's nominal capacity will be significantly overestimated due to the different power requirements during the first 6 hours of the day. These results show how a random or arbitrary choice of the day for the sizing study can lead to storage characteristics, which will not be suitable for most days. For sizing the flywheel for power smoothing applications, no significant difference between the patterns is observed, as shown in Table IV, since the high-frequency components above the filter's cut-off frequency have been more or less consistent in all patterns for this specific case.

C. The effect of data aggregation

As shown in Table III, the storage characteristics were calculated using both the 1-s and 1-min data. It can be observed that for sizing the battery, using the 1-min data leads to a notable overestimation or underestimation of its nominal power and capacity. However, this slight error might be acceptable for some applications, such as peak shaving, particularly considering the reserved lifetime-related capacity. However, for sizing flywheels (or any other high power density ESS) for power smoothing applications, using the 1-s data is mandatory. According to Table III when using 1-min data, almost twice the required capacity for buses 3 and 4 is required, which is an extreme oversizing of the flywheel, considering its high capital costs per unit of energy [36]. Moreover, the rated power of the flywheel is also largely underestimated using the 1-min data, particularly for buses 1 and 2, which have a higher share of high-frequency components. It is also important to note that in both storage technologies, the maximum ramp rate and the number of mode changes cannot be accurately calculated using the 1-min data. While an accurate estimation of these values is irrelevant for the flywheel, they are required for estimating the effective lifetime of the Li-ion battery [38].

V. EVALUATION OF THE PROPOSED SIZING METHOD

In order to evaluate the proposed sizing approach, the effectiveness of the hybrid ESS with its characteristics derived from the standard patterns only is evaluated during the period of the whole data set (14 days) for its intended applications. That is to say that the calculated nominal capacity, power, maximum ramp rate, and also maximum and minimum SOC are considered as the system constraints for charging and discharging of the battery and the flywheel. It is important to note that since the storage characteristics were derived from the 80%-quantile of the most recurring pattern and the most recurring pattern is not repeated exactly on each and every day, the ESS might not be able to fulfil its purposes during all the days during the whole data set. Nevertheless, the ESS should support the grid for the intended applications during most of the days during the whole data set, which is the main advantage of the proposed sizing method using the standard patterns, in contrast to an arbitrary choice of a typical day.

Fig. 10 shows the power drawn from the medium voltage grid at bus 4 in the following three cases:

- **Case 1**: No ESS is installed.
- **Case 2**: Only a Li-ion battery is installed for peak shaving application and reducing the reverse power flow.
- **Case 3**: The Li-ion battery is complemented by a flywheel to form a hybrid battery-flywheel ESS.

It can be observed from Fig. 10(a) that both the morning and the evening peaks in demand are eliminated for most of the days within the two weeks. The exceptions are the last few days when there is no sufficient PV generated power to fully charge the battery (see Fig. 11), where the minimum SOC limit is quickly reached. Here, using the Li-ion battery ESS can potentially defer grid expansions or relieve grid congestion, if applicable. Moreover, for most of the days (10 out of 14), the power profile no longer resembles a typical *duck curve* [39], reducing the need for flexible power plants with a high ramp capability to supply the evening increase in the demand.

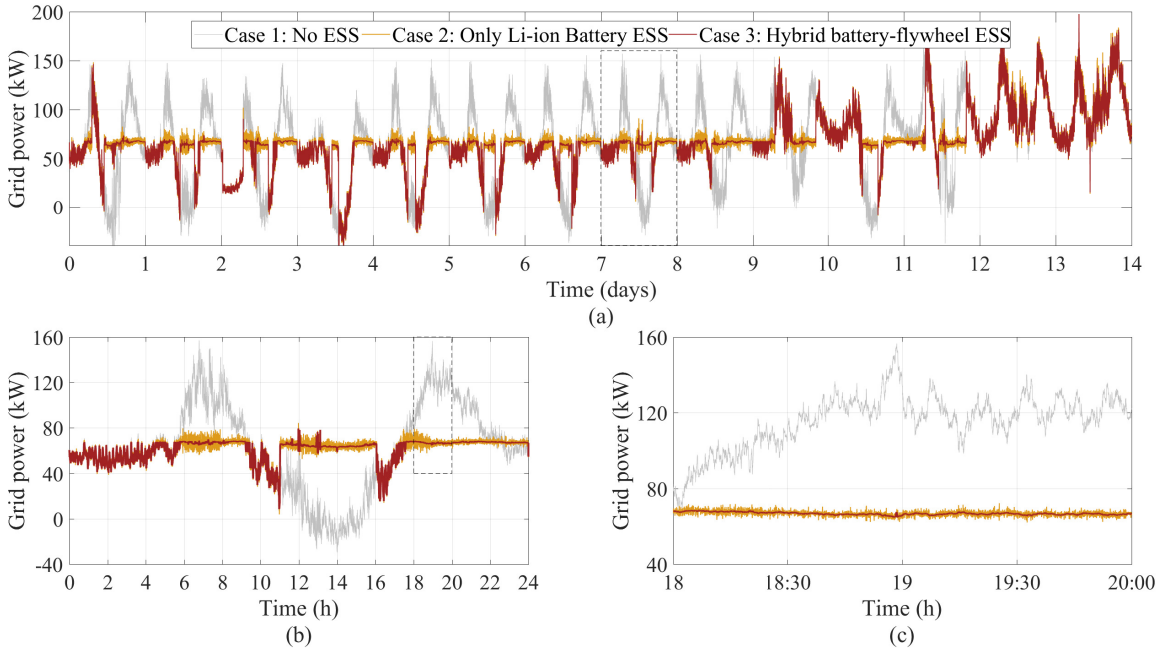

Fig. 10. The active power drawn from the medium voltage grid at bus 4 in the three different cases during (a) two weeks, (b) the 8th day, and (c) between 18:00 and 20:00 (peak hours) of the 8th day.

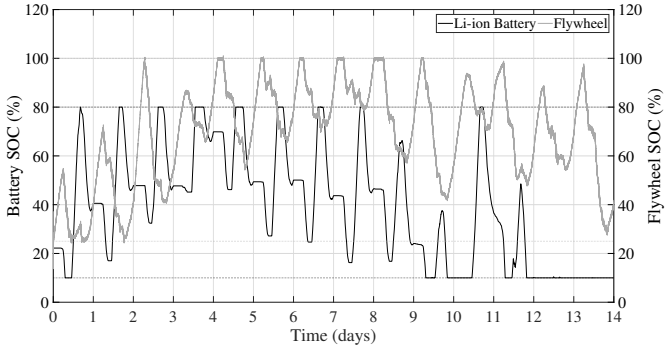

Fig. 11. The variations in the SOC of the battery and the flywheel during the studied two weeks. Dashed lines indicated the minimum and maximum permissible SOC.

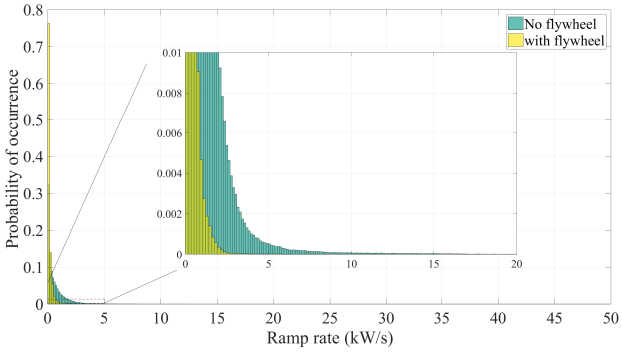

Fig. 12. The histogram of the probability of the non-zero values of the power ramp rate in case 1 and 3, i.e., cases with and without the flywheel.

If a flywheel is added to form the hybrid ESS, most short-term power fluctuations are compensated using the flywheel. This is also shown in Fig. 12, which shows the histogram of the non-zero values of the power ramp rate with and without the flywheel during two weeks, normalized according to their probability of occurrence. It can be seen that the use of the flywheel significantly reduces the probability of occurrences of high ramp rate values in the active power,up to the point that ramp rates of higher than 4 kW/s are no longer present, when using the flywheel. Without the flywheel, the high-frequency components are either drawn from the grid, as shown in Fig. 10(c) as case 2, which can lead to fast voltage changes in the grid, or they have to be covered by the Li-ion battery, leading to possible premature ageing of the battery. It should also be noted that as seen in Fig. 11, the proposed sizing approach is also effective, when the sizing of only a Li-ion battery is required for peak shaving applications, as it is commonly the case in practice.

It can be concluded that the hybrid ESS, sized using the motif discovery algorithm and the most recurring pattern, can effectively fulfil their intended grid support functionalities for most of the days at bus 4 during the studied period, showing the effectiveness of the proposed sizing approach. Similar results have been achieved for the other three buses. It is evident that with a random selection of one day for the sizing calculations, as commonly found in literature [6], [7], [13]–[15], these results cannot be achieved. For instance, if one of the last three days for bus 4 in Fig. 10 is selected for the sizing, it is clear that the sizing outcome will not be useable for the remaining days of the time series. It should also be noted that since the storage sizing is done using summer data, it is expected that the calculated sizing outcome would be

more than sufficient for the rest of the year for buses with a high share of PV generation (bus 3 and 4).

VI. Conclusion

In this paper, a new approach for sizing hybrid energy storage systems based on historical measurement data is introduced. In the first step, an improved motif discovery algorithm is developed and applied to reduce the data size by finding the most recurring consumption pattern at several low voltage grids in southern Germany. The derived standard patterns for each low voltage grid were used to represent the whole data set to derive the characteristics of a battery-flywheel hybrid ESS. Next, a simple optimization framework was introduced to find the optimum cut-off frequency of the filter to separate the power profile of each storage technology and calculate the characteristics of the hybrid ESS. Finally, it was demonstrated that the hybrid battery-flywheel ESS, with the characteristics derived from the standard patterns only, can provide the intended grid services for most of the days during the studied period, reflecting the advantage of using the motif discovery algorithm.

The improved motif discovery algorithm introduced in this paper can be applied to ease the computation of any sizing study and optimizations, e.g., sizing distributed energy storage systems and other storage technologies, by finding repeating patterns in the time series.

References

[1] T. Stetz, F. Marten, and M. Braun, "Improved low voltage grid-integration of photovoltaic systems in Germany," *IEEE Transactions on Sustainable Energy*, vol. 4, no. 2, pp. 534–542, 2013.

[2] "DIN EN 50160 - Voltage characteristics of electricity supplied by public electricity networks," VDE, DKE Deutsche Kommission Elektrotechnik Elektronik Informationstechnik, Berlin, Tech. Rep., 2011.

[3] S. Hashemi and J. Østergaard, "Efficient Control of Energy Storage for Increasing the PV Hosting Capacity of LV Grids," *IEEE Transactions on Smart Grid*, vol. 9, no. 3, pp. 2295–2303, 2018.

[4] Y. Yang, S. Bremner, C. Menictas, and M. Kay, "Battery energy storage system size determination in renewable energy systems: A review," *Renewable and Sustainable Energy Reviews*, vol. 91, no. August 2018, pp. 109–125, 2018.

[5] N. D. Hatziargyriou, D. Škrlec, T. Capuder, P. S. Georgilakis, and M. Zidar, "Review of energy storage allocation in power distribution networks: applications, methods and future research," *IET Generation, Transmission & Distribution*, vol. 10, no. 3, pp. 645–652, 2016.

[6] D. B. W. Abeywardana, B. Hredzak, V. G. Agelidis, and G. D. Demetriades, "Supercapacitor sizing method for energy-controlled filter-based hybrid energy storage systems," *IEEE Transactions on Power Electronics*, vol. 32, no. 2, pp. 1626–1637, 2017.

[7] S. Majumder, S. A. Khaparde, A. P. Agalgaonkar, P. Ciufo, S. Perera, and S. V. Kulkarni, "DFT-Based Sizing of Battery Storage Devices to Determine Day-Ahead Minimum Variability Injection Dispatch with Renewable Energy Resources," *IEEE Transactions on Smart Grid*, vol. 10, no. 1, pp. 626–638, 2019.

[8] R. C. Dugan, J. A. Taylor, and D. Montenegro, "Energy Storage Modeling for Distribution Planning," *IEEE Transactions on Industrial Applications*, vol. 53, no. 2, pp. 954–962, 2017.

[9] L. Barelli, D. A. Ciupageanu, A. Ottaviano, D. Pelosi, and G. Lazaroiu, "Stochastic power management strategy for hybrid energy storage systems to enhance large scale wind energy integration," *Journal of Energy Storage*, vol. 31, p. 101650, 2020. [Online]. Available: https://doi.org/10.1016/j.est.2020.101650

[10] N. Nguyen-Hong, H. Nguyen-Duc, and Y. Nakanishi, "Optimal Sizing of Energy Storage Devices in Isolated Wind-Diesel Systems Considering Load Growth Uncertainty," *IEEE Transactions on Industry Applications*, vol. 54, no. 3, pp. 1983–1991, 2018.

[11] P. Fortenbacher, M. Zellner, and G. Andersson, "Optimal sizing and placement of distributed storage in low voltage networks," in *19th Power Systems Computation Conference, PSCC 2016*, Genoa, Italy, 2016.

[12] K. Baker, G. Hug, and X. Li, "Optimal storage sizing using two-stage stochastic optimization for intra-hourly dispatch," in *2014 North American Power Symposium, NAPS 2014*, Pullman, WA, USA, 2014.

[13] Y. Xiang, W. Han, J. Zhang, J. Liu, and Y. Liu, "Optimal Sizing of Energy Storage System in Active Distribution Networks Using Fourier-Legendre Series Based State of Energy Function," *IEEE Transactions on Power Systems*, vol. 33, no. 2, pp. 2313–2315, 2018.

[14] F. Kazhamiaka, Y. Ghiassi-Farrokhfal, S. Keshav, and C. Rosenberg, "Comparison of Different Approaches for Solar PV and Storage Sizing," *IEEE Transactions on Sustainable Computing*, vol. Early Access, 2019.

[15] A. Oudalov, R. Cherkaoui, and A. Beguin, "Sizing and optimal operation of battery energy storage system for peak shaving application," *2007 IEEE Lausanne PowerTech*, pp. 621–625, 2007.

[16] A. Nagarajan and R. Ayyanar, "Design and Strategy for the Deployment of Energy Storage Systems in a Distribution Feeder With Penetration of Renewable Resources," *IEEE Transactions on Sustainable Energy*, vol. 6, no. 3, pp. 1085–1092, 2015.

[17] M. Nick, R. Cherkaoui, and M. Paolone, "Optimal allocation of dispersed energy storage systems in active distribution networks for energy balance and grid support," *IEEE Transactions on Power Systems*, vol. 29, no. 5, pp. 2300–2310, 2014.

[18] D. D. Sharma, S. N. Singh, B. S. Rajpurohit, and F. G. Longatt, "Critical load profile estimation for sizing of battery storage system," in *IEEE Power and Energy Society General Meeting 2015*. Denver, CO, USA: IEEE, 2015, pp. 9–13.

[19] P. D. Brown, J. A. Peças Lopes, and M. A. Matos, "Optimization of pumped storage capacity in an isolated power system with large renewable penetration," *IEEE Transactions on Power Systems*, vol. 23, no. 2, pp. 523–531, 2008.

[20] S. Karrari, N. Ludwig, V. Hagenmeyer, and M. Noe, "A method for sizing centralised energy storage systems using standard patterns," in *2019 IEEE Milan PowerTech, PowerTech 2019*, Milan, 2019.

[21] B. Chiu, E. Keogh, and S. Lonardi, "Probabilistic discovery of time series motifs," in *Proceedings of the Ninth ACM SIGKDD International Conference on Knowledge Discovery and Data Mining*, Washington, D.C., 2003, p. 493498.

[22] J. Buhler and M. Tompa, "Finding motifs using random projections," *Journal of Computational Biology*, vol. 9, no. 2, pp. 225–242, 2002.

[23] N. Ludwig, S. Waczowicz, R. Mikut, and V. Hagenmeyer, "Assessment of unsupervised standard pattern recognition methods for industrial energy time series," in *Proceedings of the Ninth International Conference on Future Energy Systems*, Karlsruhe, Germany, 2018, pp. 434–435.

[24] S. Karrari, M. Vollmer, G. De Carne, M. Noe, K. Böhm, and J. Geisbüsch, "A data-driven approach for estimating relative voltage sensitivity," in *2020 IEEE Power Energy Society General Meeting (PESGM)*, 2020.

[25] "Power Quality-Interface and Disturbance Recorder PQI-DA smart - A. Eberle GmbH & Co.KG." [Online]. Available: https://www.a-eberle.de/en/product-groups/pq-fix-installed/devices/pqi-da-smart

[26] C. Cassisi, M. Aliotta, A. Cannata, P. Montalto, D. Patanè, A. Pulvirenti, and L. Spampinato, "Motif Discovery on Seismic Amplitude Time Series: The Case Study of Mt Etna 2011 Eruptive Activity," *Pure and Applied Geophysics*, vol. 170, no. 4, pp. 529–545, 2013.

[27] E. F. Gomes, A. M. Jorge, and P. J. Azevedo, "Classifying heart sounds using multiresolution time series motifs: An exploratory study," in *Proceedings of the International C* Conference on Computer Science and Software Engineering*, Porto, Portuga, 2013, p. 2330.

[28] N. Ludwig, L. Barth, D. Wagner, and V. Hagenmeyer, "Industrial demand-side flexibility: A benchmark data set," in *Proceedings of the Tenth ACM International Conference on Future Energy Systems*, Phoenix, AZ, USA, 2019, p. 460473.

[29] J. Hou, J. Sun, and H. Hofmann, "Control development and performance evaluation for battery/flywheel hybrid energy storage solutions to mitigate load fluctuations in all-electric ship propulsion systems," *Applied Energy*, vol. 212, pp. 919–930, 2018.

[30] V. Arzamasov, R. Schwerdt, S. Karrari, K. Böhm, and T. B. Nguyen, "Privacy measures and storage technologies for battery-based load hiding - an overview and experimental study," in *Proceedings of the Eleventh ACM International Conference on Future Energy Systems*, Virtual Event, Australia, 2020, p. 178195.

[31] P. Keil, "Aging of Lithium-Ion Batteries in Electric Vehicles," PhD Thesis, Technische Universität München, 2017.

[32] S. Karrari, H. R. Baghaee, G. De Carne, M. Noe, and J. Geisbuesch, "Adaptive Inertia Emulation Control for High-speed Flywheel Energy

Storage Systems," *IET Generation, Transmission & Distribution*, vol. 14, no. 22, pp. 5047–5059, 2020.
[33] J. Xiao, L. Bai, F. Li, H. Liang, and C. Wang, "Sizing of energy storage and diesel generators in an isolated microgrid Using Discrete Fourier Transform (DFT)," *IEEE Transactions on Sustainable Energy*, vol. 5, no. 3, pp. 907–916, 2014.
[34] Y. V. Makarov, P. Du, M. C. W. Kintner-Meyer, C. Jin, and H. F. Illian, "Sizing energy storage to accommodate high penetration of variable energy resources," *IEEE Transactions on Sustainable Energy*, vol. 3, no. 1, pp. 34–40, 2012.
[35] I. N. Moghaddam and B. Chowdhury, "Optimal sizing of Hybrid Energy Storage Systems to mitigate wind power fluctuations," in *IEEE Power and Energy Society General Meeting*. Boston, MA, USA: IEEE, 2016.
[36] K. R. Pullen, "The Status and Future of Flywheel Energy Storage," *Joule*, vol. 3, no. 6, pp. 1394–1399, 2019.
[37] International Renewable Energy Agency (IRENA), "Electricity storage and renewables: Costs and markets to 2030," IRENA, Tech. Rep., 2017. [Online]. Available: www.irena.org
[38] J. Martins, S. Spataru, D. Sera, D.-I. Stroe, and A. Lashab, "Comparative study of ramp-rate control algorithms for pv with energy storage systems," *Energies*, vol. 12, no. 7, 2019.
[39] Q. Hou, N. Zhang, E. Du, M. Miao, F. Peng, and C. Kang, "Probabilistic duck curve in high PV penetration power system: Concept, modeling, and empirical analysis in China," *Applied Energy*, vol. 242, pp. 205–215, 2019.

Shahab Karrari (M09) was born in London, U.K., in 1990. He received his B.Sc. and M.Sc. degree in electrical power engineering from Amirkabir University of Technology (Tehran Polytechnic), in 2012 and 2014, respectively. In 2021, he was awarded a PhD degree (summa cum laude) from the Karlsruhe Institute of Technology (KIT) in Germany for his work on the integration of energy storage systems using real-time simulations. Since 2022, he is working at Siemens Energy as a control expert, working on advanced grid support functionality of HVDC converter stations. His main research interests include power system dynamics and control, energy storage systems, HVDC control, and hardware-in-the-loop testing.

Nicole Ludwig received her PhD in Computer Science from Karlsruhe Institute of Technology (Germany). She is an early-career research group leader within the Cluster of Excellence Machine Learning at the University of Tbingen, where her main research interests are (probabilistic) forecasting, uncertainty quantification and pattern recognition in energy time series.

Giovanni De Carne (S'14-M'17-SM'21) received the B.Sc. and M.Sc. degrees in electrical engineering from the Polytechnic University of Bari, Italy, in 2011 and 2013, respectively, and the Ph.D. degree from the Chair of Power Electronics, Kiel University, Germany, in 2018. He was a post-doctoral fellow at Kiel University, working on HVdc control and services until 2019. He is currently the head of the Real Time System Integration Group and head of the "Power Hardware In the Loop Lab" at the Institute for Technical Physics at the Karlsruhe Institute of Technology. In 2020, Dr.-Ing. De Carne has been awarded with the Helmholtz "Young Investigator Group" for the project "Hybrid Networks: a multi-modal design for the future energy system". He has authored/co-authored more than 60 peer-reviewed scientific papers. His research interests include power electronics transformers, real time modelling, and power hardware in the loop. He is the Chairman of the IEEE PES Task Force on "Solid State Transformer integration in distribution grids". He is an Associate Editor of the IEEE Industrial Electronics Magazine and IEEE Open Journal of Power Electronics.

Mathias Noe has received his M.S. in Power Engineering in 1991 and his Ph.D. in 1998, both from the University of Hanover in Germany. After a Postdoc position at the Ecole Polytechnic Federale de Lausanne in Switzerland, he joined Forschungszentrum Karlsruhe in 1998 and became later group leader for high temperature superconducting power devices at the Institute for Technical Physics. Since 2006 he is director of the Institute for Technical Physics at the Karlsruhe Institute of Technology and full professor for technical applications of high temperature superconductivity at the faculty of electrical engineering and information technology.Prof. Noe is active in the field of new energy technology and applied superconductivity since 1991 and is the author of more than 100 reviewed articles in this field. Recently, he was spokesperson of the Helmholtz Program Energy Storage and cross-linked Infrastructure and Coordinator of the EERA Joint Program Energy Storage. In addition, he is member of several boards, panels and committees in his research field, among them he served from 2011-2015 as a president of the European Society of Applied Superconductivity.